

Stephens, R.D.; Warner, B.D. (2018). “Lightcurve Analysis of L5 Trojan Asteroids at the Center for Solar System Studies: 2018 January to March.” *Minor Planet Bull.* **45**, 301-304.

Thirouin, A.; Ortiz, J. L.; Duffard, R.; Santos-Sanz, P.; Aceituno, F.J.; Morales, N. (2010). “Short-term variability of a sample of 29 trans-Neptunian objects and Centaurs.” *Astro. and Astro.* **522** A93.

Tonry, J.L.; Denneau, L.; Flewelling, H.; Heinze, A.N.; Onken, C.A.; Smartt, S.J.; Stalder, B.; Weiland, H.J.; Wolf, C. (2018). “The ATLAS All-Sky Stellar Reference Catalog.” *Astrophys. J.* **867**, A105.

Warner, B.D.; Harris, A.W.; Pravec, P. (2009). “The Asteroid Lightcurve Database.” *Icarus* **202**, 134-146. Updated 2019 Feb. <http://www.minorplanet.info/lightcurvedatabase.html>

## SPIN-SHAPE MODEL FOR 131 VALA

Lorenzo Franco  
Balzaretto Observatory (A81), Rome, ITALY  
lor\_franco@libero.it

Frederick Pilcher  
4438 Organ Mesa Loop  
Organ Mesa Observatory (G50)  
Las Cruces, NM 88011 USA

Alessandro Marchini  
Astronomical Observatory, DSFTA - University of Siena (K54)  
Via Roma 56, 53100 - Siena, ITALY

Giorgio Baj  
M57 Observatory (K38), Saltrio, ITALY

Paolo Bacci, Martina Maestripietri  
San Marcello Pistoiese (104), Pistoia, ITALY

Roberto Bacci  
G. Pascoli Observatory (K63), Castelveccchio Pascoli, ITALY

(Received: 2019 June 22 Revised: 2019 August 2)

We present shape and spin axis model results for main-belt asteroid 131 Vala. The model was achieved with the lightcurve inversion process, using combined dense photometric data acquired from four apparitions, between 2007-2018 and sparse data from USNO Flagstaff. Analysis of the resulting data found a sidereal period  $P = 5.180810 \pm 0.000023$  h and two mirrored pole solutions at  $\lambda = 54^\circ$ ,  $\beta = 29^\circ$  and  $\lambda = 243^\circ$ ,  $\beta = 30^\circ$  with an uncertainty of  $\pm 15$  degrees.

We report that minor planet 131 Vala was recently observed in order to acquire data for lightcurve inversion work (Franco et al., 2019). A search in the asteroid lightcurve database (LCDB; Warner et al., 2009) shows many entries, covering a wide range of phase angle bisectors. Dense photometric data were downloaded from ALCDEF (ALCDEF, 2019) and sparse data instead were taken from the Asteroids Dynamic Site (AstDyS-2, 2018).

The observational details of the dense data used are reported in Table I with the mid date of the observing campaign, longitude and latitude of phase angle bisector ( $L_{PAB}$ ,  $B_{PAB}$ ).

Reference	Mid date	PABL $^\circ$	PABB $^\circ$
Pilcher (2008)	2007-10-22	48	-2
Pilcher (2009)	2009-02-18	167	7
Pilcher (2017)	2017-06-04	231	1
Franco et al. (2019)	2018-09-28	6	-6

Table I. Observational details for the data used in the lightcurve inversion process for 131 Vala.

Lightcurve inversion was performed using *MPO LCInvert* v.11.7.5.1 (BDW Publishing, 2016). For a description of the modeling process see *LCInvert Operating Instructions Manual* and Warner et al. (2017).

In order to find a better solution, we have also used sparse data from USNO Flagstaff Station (MPC Code 689) in addition to the dense data. Figure 1 shows the wide PAB longitude/latitude distribution for dense/sparse data used in the lightcurve inversion process. Figure 2 (top panel) shows the sparse photometric data

distribution (intensities vs JD) and (bottom panel) the corresponding phase curve (reduced magnitudes vs phase angle).

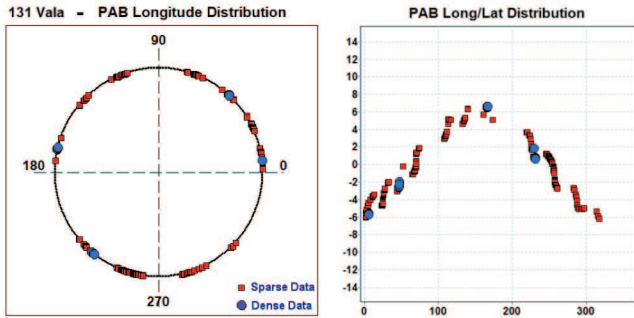


Figure 1: PAB longitude and latitude distribution of the data used for the lightcurve inversion model.

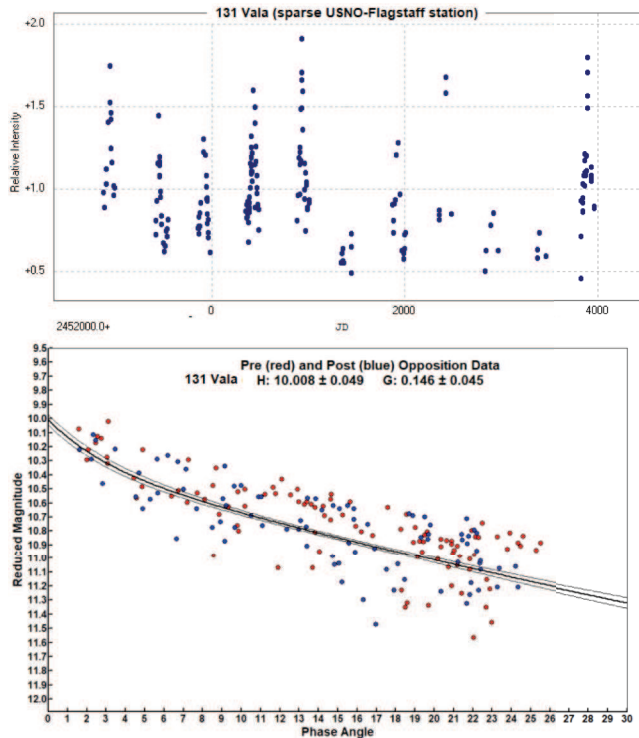


Figure 2: Top: sparse photometric data point distribution from (689) USNO Flagstaff station (relative intensity of the asteroid's brightness vs Julian Day). Bottom: phase curve obtained from sparse data (reduced magnitude vs phase angle).

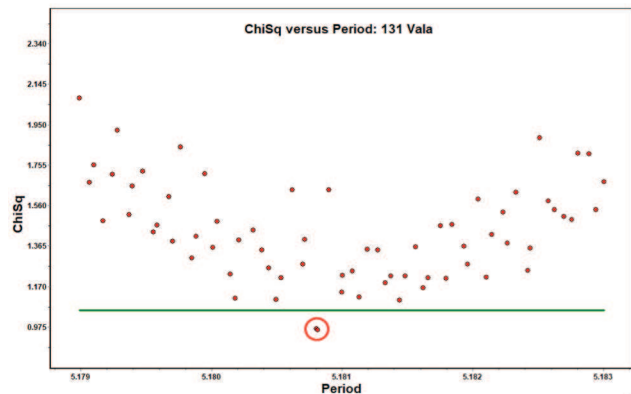


Figure 3: The period search for 131 Vala shows two overlapping sidereal periods with Chi-Sq values within 10% of the lowest value.

In the analysis the processing weighting factor was set to 1.0 for dense data and to 0.3 for sparse data. The “dark facet” weighting factor was set to 2.0 to keep the dark facet area below 1% of total area and the number of iterations was set to 50.

The sidereal period search was started around the average of the synodic periods found in the asteroid lightcurve database (LCDB; Warner et al., 2009). We found two very close sidereal periods within 0.000012 hours with a Chi-Sq value within 10% of the lowest Chi-Sq (Figure 3). Of these was chosen the one with the lowest Chi-Sq value.

The pole search was started using the “medium” option with the previously found sidereal period set to “float”. From this step we found two roughly mirrored lower Chi-Sq solutions (Figure 4) separated by 180° in ecliptic longitude, (60°, 15°) and (240°, 30°).

The subsequent “fine” search that was centered on these rough positions, allowed us to refine the position of the pole (Figure 5). The analysis shows two clustered solutions of ecliptic longitude-latitude pairs within 15° of radius that had Chi-Sq values within 10% of the lowest value.

The two best solutions (lowest two Chi-Sq values) are reported in Table II. The sidereal period was obtained by averaging the two solutions found in the pole search process. Typical errors in the pole solution are ± 15° and the uncertainty in sidereal period has been evaluated as a rotational error of 30° over the total time span of the dense data set. Figure 6 shows the shape model (first solution) while Figure 7 shows the fit between the model (black line) and some observed lightcurves (red points).

$\lambda^\circ$	$\beta^\circ$	Sidereal Period (hours)	RMS
54	29	$5.180810 \pm 0.000023$	0.0151
243	30		0.0153

Table II. The two spin axis solutions for 131 Vala (ecliptic coordinates). The sidereal period was the average of the two solutions found in the pole search process.

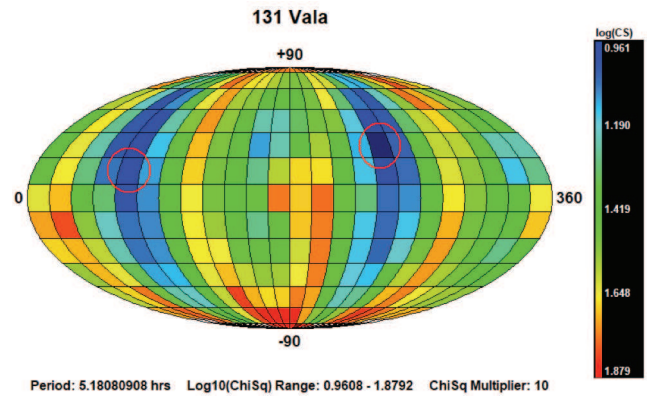


Figure 4: Pole search distribution. The dark blue indicates the better solutions (lower Chi-Sq), while maroon the worst ones.

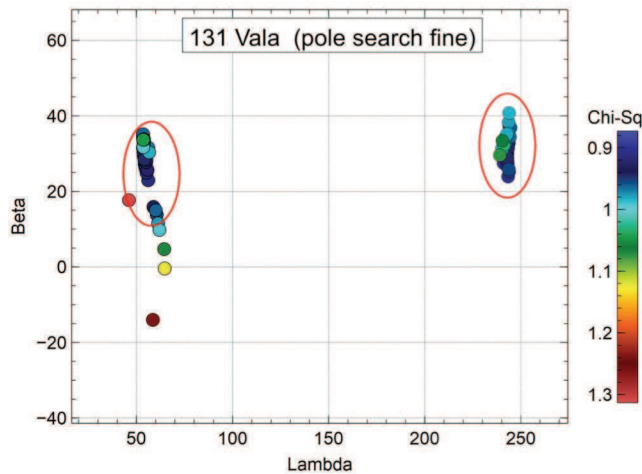


Figure 5: The “fine” pole search shows two clustered solutions centered at the ecliptic longitude/latitude ( $54^\circ$ ,  $30^\circ$ ) and ( $243^\circ$ ,  $31^\circ$ ) with radius approximately of  $10^\circ$  and Chi-Sq values within 10% of the lowest value.

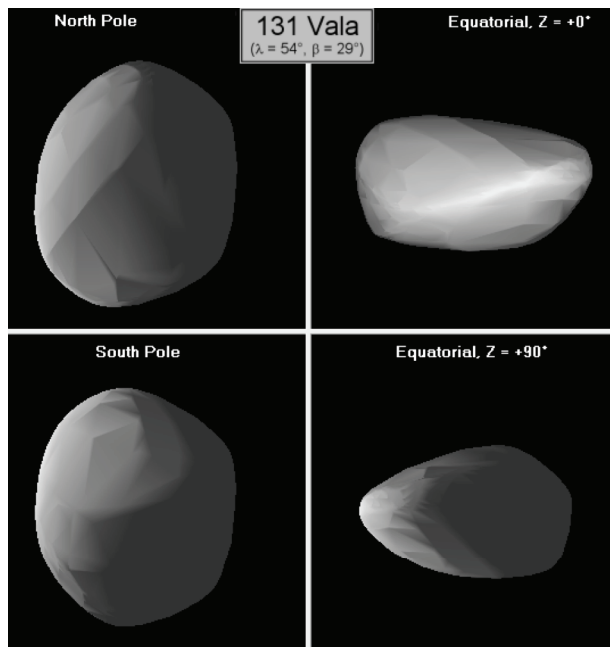


Figure 6: The shape model for 131 Vala ( $\lambda = 54^\circ$ ,  $\beta = 29^\circ$ ).

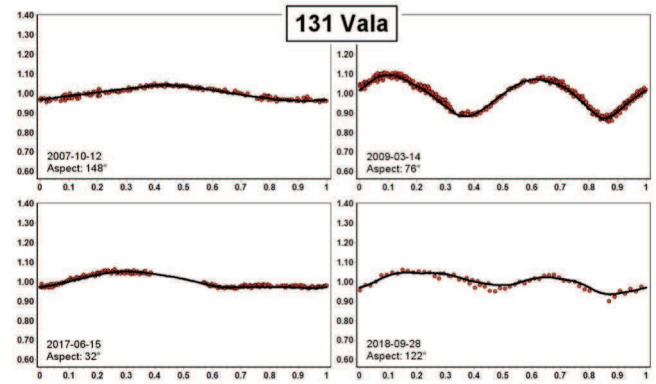


Figure 7: Model fit (black line) versus observed lightcurves (red points) for ( $\lambda = 54^\circ$ ,  $\beta = 29^\circ$ ) solution.

## References

- ALCDEF (2019). Asteroid Lightcurve Data Exchange Format web site. <http://www.alcdef.org/>
- AstDyS-2 (2018), Asteroids - Dynamic Site. <http://hamilton.dm.unipi.it/astdys/>
- BDW Publishing (2016). <http://www.minorplanetobserver.com/MPOSoftware/MPOLCInvert.htm>
- DSFTA (2019). Dipartimento di Scienze Fisiche, della Terra e dell'Ambiente – Astronomical Observatory. <https://www.dsfta.unisi.it/en/research/labs-eng/astronomical-observatory>
- Franco, L.; Marchini, A.; Baj, G.; Scarfi, G.; Bacci, P.; Maestripieri, M.; Bacci, R.; Papini, R.; Salvaggio, F.; Banfi, M. (2019). “Lightcurves for 131 Vala, 374 Burgundia, 734 Brenda, and 929 Algunde.” *Minor Planet Bulletin* **46**, 86-86.
- Pilcher, F. (2008). “Period Determination for 84 Klio, 98 Ianthe, 102 Miriam 112 Iphigenia, 131 Vala, and 650 Amalasantha.” *Minor Planet Bulletin* **35**, 71-72.
- Pilcher, F. (2009). “Rotation Period Determinations for 120 Lachesis, 131 Vala 157 Dejanira, and 271 Penthesilea.” *Minor Planet Bulletin* **36**, 100-102.
- Pilcher, F. (2017). “Lightcurves of 131 Vala and 612 Veronika During Their 2017 Apparitions.” *Minor Planet Bulletin* **44**, 317-318.
- Warner, B.D.; Harris, A.W.; Pravec, P. (2009). “The asteroid lightcurve database.” *Icarus* **202**, 134-146. Updated 2019 January. <http://www.minorplanet.info/lightcurvedatabase.html>
- Warner, B.D.; Pravec, P.; Kusnirak, P.; Benishek, V.; Ferrero, A. (2017). “Preliminary Pole and Shape Models for Three Near-Earth Asteroids.” *Minor Planet Bulletin* **44**, 206-212.